Noise-resolution trade-off in projection algorithms for laser diffraction particle sizing

Francisco Pedocchi and Marcelo H. García

The size distribution of a particle suspension can be inferred from studying the diffracted light pattern produced by a laser beam that passes through the suspension. This involves solving an ill-posed linear system. Two previous versions of projection algorithms were tested by use of computer simulations and experiments. Both algorithms showed limitations in restoring the size distribution, because of either the shape of the size distribution or the presence of noise in the scattered light signal. The generalized projection algorithm presented in this work solves these difficulties by introducing a parameter that allows the user to adjust the noise-resolution trade-off, making it suitable for the analysis of natural suspensions.

OCIS codes: 100.3190, 290.5850, 010.4450, 350.4990.

1. Introduction

A. Natural Particles and Laser Diffraction

In the past few years, the use of laser diffraction for particle sizing has expanded to many new fields of knowledge. In particular, in the past decade laser diffraction has begun to be applied to sediment transport research in natural water bodies.[1] In these natural environments the type and size distribution of particles continuously change and no hypothesis on the shape of the size distribution can be made in advance.

The physical bases of laser diffraction application for particle sizing can be briefly explained as follows. When light rays meet a suspended particle, they are diffracted over all spatial directions. The rays that do not enter into the particle, but pass close to it, are diffracted at small angles in a pattern characteristic of each particle size.[2] If the particle is larger than the wavelength of the laser, the refractive index of the particles will not affect the light scattering and the particle will diffract the light as if it were a small aperture. Under these conditions all the light scattered at small angles is assumed to be due to diffraction. For a suspension composed of many particles, the size distribution of the suspension can be inferred from their combined diffracted light pattern.

An important restriction to the practical applications of laser diffraction for particles sizing is avoiding multiple light scattering. This means that the light rays must be diffracted only one time as they travel from the light source to the light detector. Although some theoretical adjustments may be done to correct the effect of multiple scattering,[3,4] the most common approach is for one to reduce the traveling path of the light through the sizing chamber by using tiny measuring volumes and working with low concentrated suspension. Unfortunately these two practical restrictions tend to drastically reduce the number of particles that are sampled, degrading the statistical confidence of the results especially for the larger sizes.

Another important restriction is the assumption that the measured particles are spheres. This particular restriction may become very important in natural environments. Mühlenweg and Hirleman[5] reported that, although the particle microstructure (its surface roughness) has no effect on the light scattering, the particle macrostructure (its axis ratio) may have an important influence on it. They suggested corrections to usual theory for spheres. However, the axis ratios of the particles should be known in advance by a three-dimensional shape analysis and a calibration for each type of particle is needed. Matsuyama *et al.*[6] discussed scattering that is due to randomly orientated ellipsoids. Their conclusions are that, if the particle size distribution is wide enough

The authors are with the Ven Te Chow Hydrosystems Laboratory, Department of Civil and Environmental Engineering, University of Illinois at Urbana-Champaign, 205 North Mathews Avenue, Urbana, Illinois 61801.

Received 15 June 2005; revised 21 September 2005; accepted 11 December 2005; posted 12 December 2005 (Doc. ID 62708).

0003-6935/06/153620-09$15.00/0

with respect to the aspect ratio of the ellipsoids and if the ellipsoids are randomly oriented, a peak will be observed at the size of the minor axis. From both works it is concluded that the scattering light will be spread over a wider range than if the particles were spheres, limiting the resolution of the size distributions that can be obtained.

In addition to these practical limitations, the mathematical inversion of the scattered light signal to restore the size distribution is still an important source of uncertainty. The inversion involves solving an ill-posed algebraic linear system in which small amounts of noise can lead to strongly oscillating solutions. The environmental application of laser diffraction for particle sizing has the additional restriction that many size distributions can be expected, making inappropriate the use of algorithms that introduce limitations on the shape or behavior of the size distribution.

B. Laser Diffraction Theory

Hirleman[7] and Gomi[3] present the main features of the single light-scattering theory. According to this theory the power distribution over small angles $E(\theta)$ of a plane wave of light that is diffracted by a sphere is given by

$$E(\theta) \equiv i(\theta)\theta \propto \frac{2J_1^2(\sigma\theta)}{\sigma\theta} D^3. \tag{1}$$

In Eq. (1), $i(\theta)$ is the intensity distribution of the diffracted light, θ is the light diffraction angle, D is the diameter of the sphere, J_1 is the first-order Bessel function, σ is a dimensionless size parameter equal to $\pi D/\lambda$, and λ is the light wavelength. The "proportional to" symbol ($\propto$) is used to avoid the use of proportionality constants.

When the particles in the measuring volume are randomly distributed and the distance between them is large compared with the light wavelength, the total diffracted power distribution is equal to the sum of powers due to the presence of individual particles. Then the power distribution of a suspension becomes

$$E(\theta) \propto \int \frac{2J_1^2(\sigma\theta)}{\sigma\theta} D^3 n(D)\mathrm{d}D, \tag{2}$$

where $n(D)$ is the number distribution of particles.

In practice this continuous power distribution is measured by a discrete number (N) of photosensitive detectors, and the discrete form of expression (2), using index notation, is

$$E_i = K_{ij} V_j, \tag{3}$$

where E_i is the power distribution over the N detectors ($i = 1, 2, \ldots, N$), V_j is the volume distribution expressed in N-size classes ($j = 1, 2, \ldots, N$),

$$V_j \propto \int_{D_{j,\min}}^{D_{j,\max}} D^3 n(D)\mathrm{d}D, \tag{4}$$

and $D_{j,\min}$ and $D_{j,\max}$ are minimum and maximum particles diameters in the jth class, respectively. The kernel matrix K_{ij} is defined as

$$K_{ij} \propto \frac{1}{(\sigma_{j,\max} - \sigma_{j,\min})} \int_{\sigma_{j,\min}}^{\sigma_{j,\max}} \int_{\theta_{i,\min}}^{\theta_{i,\max}} \frac{2J_1^2(\sigma\theta)}{\sigma\theta}\, \mathrm{d}\theta\mathrm{d}\sigma. \tag{5}$$

The developer (Sequoia Scientific, Inc.) of our particle size analyzer (LISST type B) provides the kernel matrix for 32 log-spaced ring-shaped detectors that allow computing the light that is diffracted by the jth class of particles into the ith detector. The kernel matrix was computed for spheres by use of the full Lorenz–Mie theory for light scattering in order to take into account the effect of the refractive index and to allow for the measurement of the scattering energy at large angles.[2]

2. Generalized Projection Algorithm

A. The Algorithm

The kernel matrix K_{ij} in Eq. (3) is ill posed. This leads to highly unstable solutions in which even low noise levels may be amplified. Riley and Agrawal[8] presented an extended discussion and comparison over many different algorithms that may be used to solve Eq. (3) in the presence of noise. One of them was the projection algorithm published by Huang *et al.*[9] in 1975 and recently revised by Jianping *et al.*[10] Both of them are presented in this section as particular cases of a generalization of the algorithm of Jianping *et al.*[10]

Equation (3) can be rewritten as a system of N equations with N unknowns[9]:

$$\begin{aligned} E_1 &= K_{11}V_1 + K_{12}V_2 + \cdots + K_{1N}V_N, \\ E_2 &= K_{21}V_1 + K_{22}V_2 + \cdots + K_{2N}V_N, \\ &\vdots \\ E_N &= K_{N1}V_1 + K_{N2}V_2 + \cdots + K_{N}V_N. \end{aligned} \tag{6}$$

In an N-dimensional space, each of the equations of the system can be thought as a plane and the solution of the system $V_j = (V_1, V_2, \ldots, V_N)$ as the intersection point of these planes. We start the first cycle of iteration by considering an initial guess $V_j^{0,1} = (V_1^{0,1}, V_2^{0,1}, \ldots, V_N^{0,1})$. We construct the next guess solution $V_j^{1,1}$ by projecting $V_j^{0,1}$ over the first plane ($E_1 = K_{11}V_1 + K_{12}V_2 + \cdots + K_{1N}V_N$), which gives

$$V_j^{1,1} = V_j^{0,1} - \left(\frac{K_{1j}V_j^{0,1} - E_1}{K_{1j}K_{1j}}\right) K_{1j}. \tag{7}$$

We construct the third guess solution by projecting $V_j^{1,1}$ into the second plane, and so on until we project over the Nth plane.

The second cycle starts with $V_j^{N,1}$ as first guess and repeating the procedure of projecting over the N planes. This process may be repeated M times until a certain condition is reached. After the last iteration, the final approximation to the solution will be $V_j^{N,M}$. In general, in one typical iteration, the projection over the Ith plane during the nth cycle will be

$$V_j^{I,n} = V_j^{(I-1),n} - \left[\frac{K_{Ij}V_j^{(I-1),n} - E_I}{K_{Ij}K_{Ij}}\right]K_{Ij}. \quad (8)$$

This algorithm converges well in the absence of noise independently of the initial solution guess. However, if noise is present it tends to amplify it as we increase the number of iterations, and there is not a general rule to define the suitable number of iteration cycles.[9]

Jianping *et al.*[10] presented a variation of this algorithm by introducing a convergence coefficient equal to $1/n$, where n is the iteration cycle number. When the convergence coefficient is used, Eq. (8) is given as

$$V_j^{I,n} = V_j^{(I-1),n} - \frac{1}{n}\left[\frac{K_{Ij}V_j^{(I-1),n} - E_I}{K_{Ij}K_{Ij}}\right]K_{Ij}. \quad (9)$$

After analyzing the capabilities of both algorithms, we discuss a generalization of the version of Jianping *et al.*[10] by setting the convergence coefficient equal to $1/n^{\alpha}$:

$$V_j^{I,n} = V_j^{(I-1),n} - \frac{1}{n^{\alpha}}\left[\frac{K_{Ij}V_j^{(I-1),n} - E_E}{K_{Ij}K_{Ij}}\right]K_{Ij}, \quad (10)$$

where α is a trade-off parameter that has to be set according to the type of size distribution and the noise levels. Note that Eqs. (8) and (9) are special cases of Eq. (10) with α equal to 0 and 1, respectively. The possible useful values of α and how they affect the restoring process of the size distribution from the scattering power are presented in the next section.

To evaluate the convergence of the algorithm, we choose a residual in the same way as Riley and Agrawal.[8] The residual is the normalized difference between the actual energy distribution E_i and the computed energy distribution $K_{ij}V_j^{I,N}$ that we obtain by using the last restored size distribution $V_j^{I,N}$:

$$R^{I,N} = \frac{\left[(E_i - K_{ij}V_j^{I,N})(E_i - K_{ij}V_j^{I,N})\right]}{(E_iE_i)} \quad \text{for } E_i \neq 0. \quad (11)$$

In Eq. (11) the use of the square was avoided in order to indicate that a summation over the index i should be performed, and the square brackets are included to emphasize that the summation should be performed in both the numerator and the denominator separately, to finally obtain a scalar.

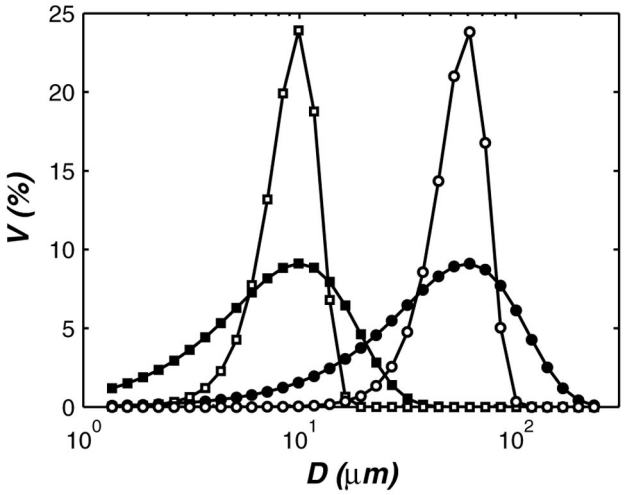

Fig. 1. Size distributions normalized with the Rosin–Rammler model with means $\overline{D}$ = 10 μm (squares) and $\overline{D}$ = 60 μm (circles) and widths δ = 1.5 (open symbols) and δ = 4 (filled symbols).

Following Jianping *et al.*[10] we compute the residual at each iteration step and compare it with its value in the previous iteration. When the difference is smaller than some preset value ε the iteration process is stopped. Symbolically the criterion to stop the iteration is

$$\left|R^{I,N} - R^{I-1,N}\right| < \varepsilon. \quad (12)$$

At the stopping point $I = M$, the final error R associated with the restored distribution will be

$$R = \frac{\left[(E_i - K_{ij}V_j^{M,N})(E_i - K_{ij}V_j^{M,N})\right]}{(E_iE_i)}. \quad (13)$$

3. Results and Discussion

A. Synthetic Size Distributions

To study how the projection algorithm works and the effect of the exponent α on the shape and stability of the solutions, we performed different computer simulations by using different modeled size distributions. The first step in this process was to create a size distribution. The Rosin–Rammler model for the particle size distribution was used in these simulations since it fits a wide variety of suspensions.

In the Rosin–Rammler model the size distribution is described by

$$V_{(x<D)} = \int_0^D V(x)\mathrm{d}x = 1 - \exp\left[-\left(\frac{D}{\overline{D}}\right)^{\delta}\right], \quad (14)$$

where $V_{(x<D)}$ is the cumulative volume fraction of particles with diameters smaller than D and $V(x)$ is the size distribution. Then the normalized volume in

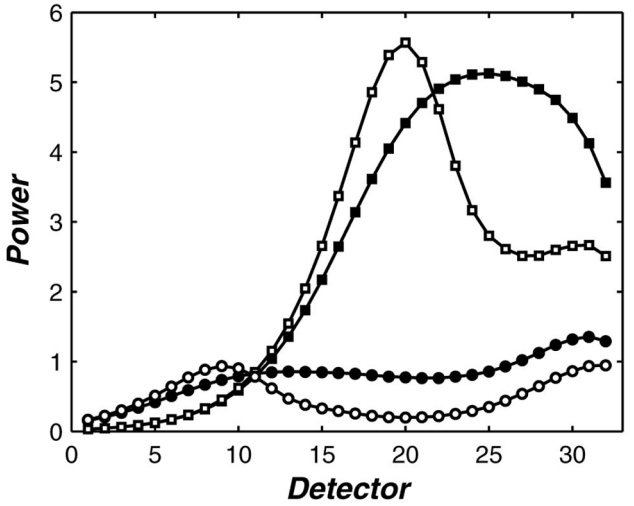

Fig. 2. Scattering power in arbitrary units over the 32 power detectors from the size distributions in Fig. 1. Symbols are the same as in Fig. 1.

each size class can be computed as

$$V_j = \exp\left[-\left(\frac{D_{j,\min}}{\overline{D}}\right)^{\delta}\right] - \exp\left[-\left(\frac{D_{j,\max}}{\overline{D}}\right)^{\delta}\right]. \quad (15)$$

$\overline{D}$ is the diameter for which $1 - 1/e = 0.6321$ fraction of the particles is smaller and δ is inversely proportional to the distribution spreading; they are referred as "mean" and "width," respectively, in the subsequent subsections.

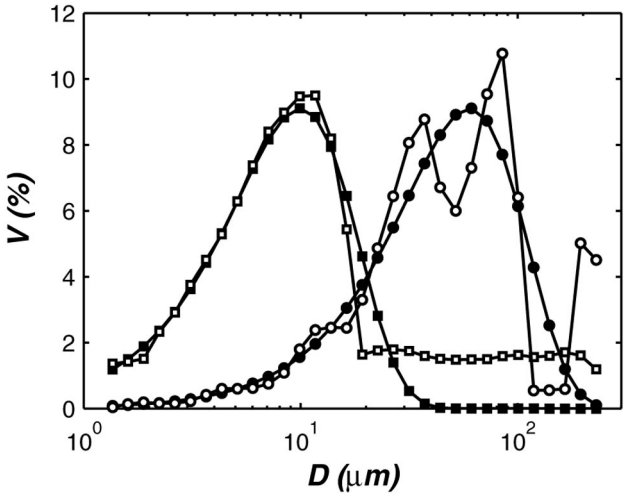

Fig. 3. Original (filled symbols) and restored (open symbols) size distributions with 3% noise added to the scattering power signal, with $\alpha = 0$. The criterion to stop the iteration was $\varepsilon = 10^{-6}$ [condition (12)]. The distributions had means $\overline{D} = 10$ μm (squares) and $\overline{D} = 60$ μm (circles) and width $\delta = 1.5$. The residual, the total number of iterations, and the relative volume were $R = 4.42 \times 10^{-4}$, $M = 21$, and $V = 1.12$ for $\overline{D} = 10$ μm, respectively, and $R = 5.20 \times 10^{-4}$, $M = 85$, and $V = 1.04$ for $\overline{D} = 60$ μm, respectively.

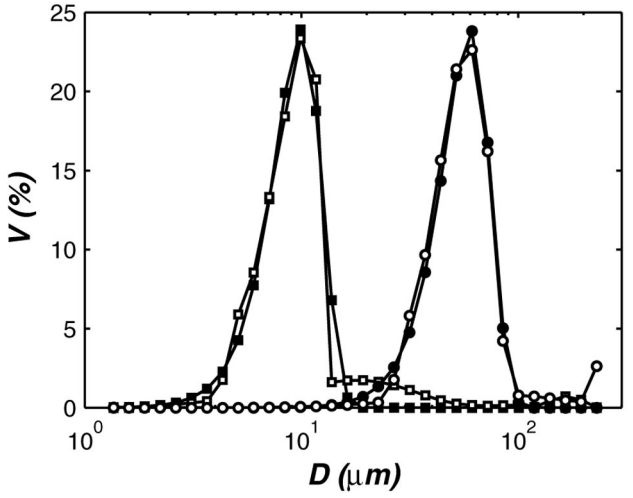

Fig. 4. Original (filled symbols) and restored (open symbols) size distributions with 3% noise added to the scattering power signal, with $\alpha = 0$. The criterion to stop the iteration was $\varepsilon = 10^{-6}$ [condition (12)]. The distributions had means $\overline{D} = 10$ μm (squares) and $\overline{D} = 60$ μm (circles) and width $\delta = 4$. The residual, the total number of iterations, and the relative volume were $R = 0.0016$, $M = 155$, and $V = 1.06$ for $\overline{D} = 10$ μm, respectively, and $R = 8.08 \times 10^{-4}$, $M = 74$, and $V = 1.04$ for $\overline{D} = 60$ μm, respectively.

B. Noise Effect and Size Distribution Width

Different size distributions may be generated by use of the Rosin–Rammler size distribution. The scattering power can be computed in each case with Eq. (3); see Figs. (1) and (2). We can then add noise to the scattering power distribution before inverting the data in order to study its effect on the restored distribution quality.

As mentioned in the introduction, many restrictions regarding laser diffraction physics are involved in its application for particle sizing. All could be considered possible noise sources that affect the uncertainty of the restored particle size distribution. Also, the electronics that are used to acquire and process the scattered power signal represent possible noise sources, affecting the data quality. Since considering each particular noise source could be a difficult task that may not produce significant results, it is common practice to study only the effects of white noise in the inversion process.[8–10]

The white-noise amplitude is expected to be independent of the scattered angle range that it is covered by each of the 32 light sensors. However, as can be observed in Fig. 2, the detectors placed at the smaller angles usually present lower power levels. Therefore a noise level selected proportional to the power of each sensor would underestimate the noise effects over the small-angle sensors. For the simulations presented here, the noise level on each ring was selected based on the total energy of the scattered light signal over all sensors.

A probability distribution for the noise should also be selected. We selected normal noise distribution after studying many actual experiments with our instrument (LISST type B). In particular, experiments

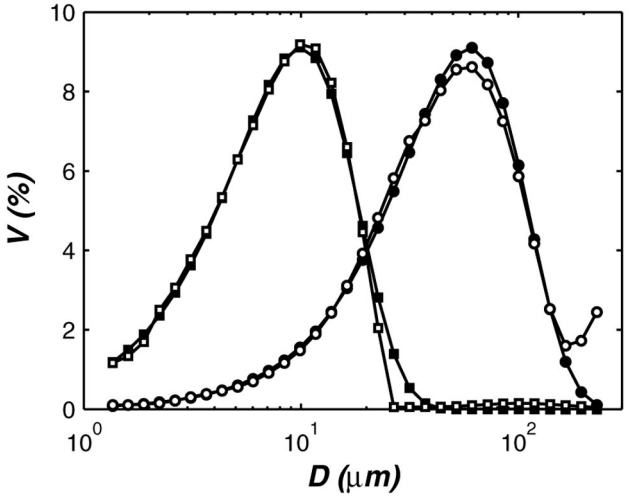

Fig. 5. Original (filled symbols) and restored (open symbols) size distributions with 3% noise added to the scattering power signal, with $\alpha = 1$. The criterion to stop the iteration was $\varepsilon = 10^{-6}$ [condition (12)]. The distributions had means $\overline{D} = 10$ μm (squares) and $\overline{D} = 60$ μm (circles) and width $\delta = 1.5$. The residual, the total number of iterations, and the relative volume were $R = 6.94 \times 10^{-4}$, $M = 31$, and $V = 0.95$ for $\overline{D} = 10$ μm, respectively, and $R = 6.97 \times 10^{-4}$, $M = 33$, and $V = 1.02$ for $\overline{D} = 60$ μm, respectively.

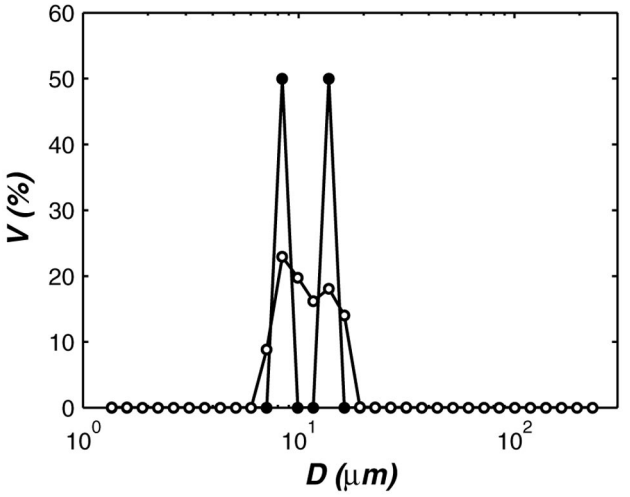

Fig. 7. Original (filled symbols) and restored (open symbols) bimodal size distributions with no noise added to the scattering power signal, with $\alpha = 0$. The criterion to stop the iteration was $\varepsilon = 10^{-6}$ [condition (12)]. Two empty size classes in between the original peaks are necessary to capture the two peaks in the restored distribution. The residual, the total number of iterations, and the relative volume were $R = 8.83 \times 10^{-4}$, $M = 264$, and $V = 1.00$, respectively.

with clear water were used as estimations of the noise that may be expected. As can be observed from the simulations and actual experiments shown in this paper, the use of a normal noise distribution on the simulations produces effects similar to the ones observed in the actual size distribution measurements. However, the use of any other probability distribution will not significantly affect the discussion presented in this paper.

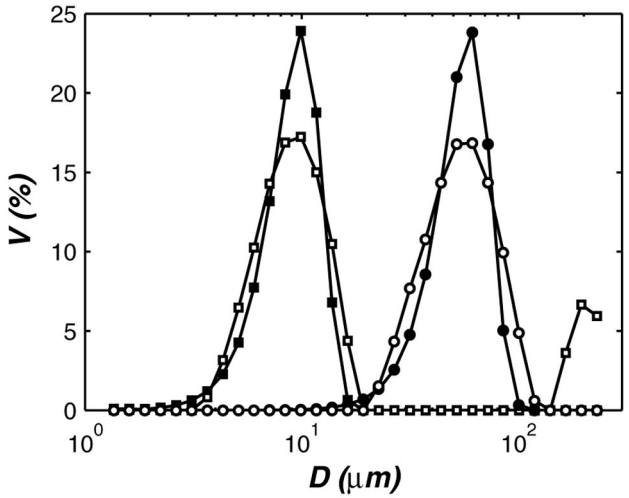

Fig. 6. Original (filled symbols) and restored (open symbols) size distributions with 3% noise added to the scattering power signal, with $\alpha = 1$. The criterion to stop the iteration was $\varepsilon = 10^{-6}$ [condition (12)]. The distributions had means $\overline{D} = 10$ μm (squares) and $\overline{D} = 60$ μm (circles) and width $\delta = 4$. The residual, the total number of iterations, and the relative volume were $R = 0.0031$, $M = 334$, and $V = 1.16$ for $\overline{D} = 10$ μm, respectively, and $R = 0.0023$, $M = 430$, and $V = 1.02$ for $\overline{D} = 60$ μm, respectively.

The noise level selected for the simulations was a percentage of the total average energy level over the 32 sensors. Figures 3–6 show results computed with a 3% noise level. This was made by a random selection of 32 numbers from a normal distribution with mean of 0 and variance of 1. Then these 32 numbers were multiplied by 0.03 times the average scattering power and added to the 32 class power signals. Finally, the size distribution was restored from the noisy scattering power signal by use of the projection algorithms. As mentioned above, the power levels over the small-angle sensors are lower and therefore the relative noise level on these sensors is higher than that on the larger-angle sensors.

Figures 3–6 show the original and the restored Rosin–Rammler distributions [relation (17)] for two different values of the mean diameter ($\bar{D} = 10$ μm and $\bar{D} = 60$ μm) and two different values of distribution width ($\delta = 1.5$ and $\delta = 4$). The restored distributions were obtained with the convergence coefficient $1/n^{\alpha}$ [Eq. (10)] for $\alpha = 0$ and $\alpha = 1$, allowing the evaluation of the performance of the algorithms presented by Huang *et al.*[9] and Jianping *et al.*[10], respectively. In addition, Figs. 3–6 also list the restoring error R [Eq. (13)] and the ratio V between the restored and the original total volume concentrations. The difference in the residuals of two consecutive iterations ε [condition (12)] was set equal to 10^{-6} for all the simulations.

We can draw these primary conclusions from the results shown in Figs. 3–6:

- The recovering of narrow distributions by use of $\alpha = 0$ is not highly affected by the presence of noise into the signal, and the narrow distribution peak is correctly solved. However, the noise is strongly am-

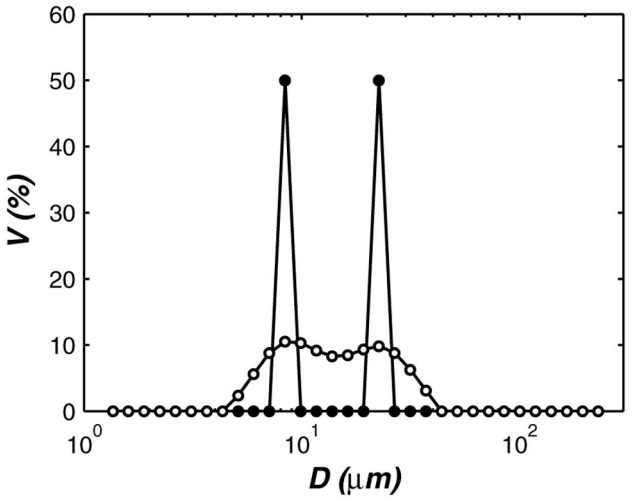

Fig. 8. Original (filled circles) and restored (open symbols) bimodal size distributions with no noise added to the scattering power signal, with $\alpha = 1$. The criterion to stop the iteration was $\varepsilon = 10^{-6}$ [condition (12)]. Five empty size classes in between the original peaks are necessary to capture the two peaks in the restored distribution. The residual, the total number of iterations, and the relative volume were $R = 0.0118$, $M = 425$, and $V = 1.01$, respectively.

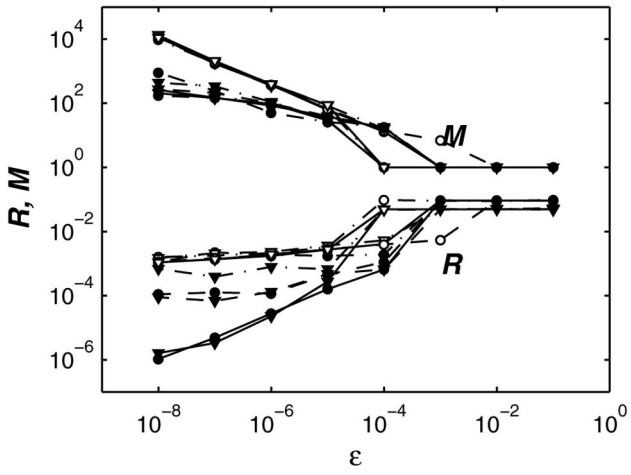

Fig. 10. Final residual R and number of iterations M as functions of the difference between two consecutive residuals ε. The size distributions have means $\overline{D} = 10$ μm (circles) and $\overline{D} = 60$ μm (triangles) and variance $\delta = 4$. The noise levels added to the power signal were 0% (solid lines), 1% (dashed lines), and 3% (dash–dotted lines). The values of α used in the restoration process were $\alpha = 0$ (filled symbols) and $\alpha = 1$ (open symbols).

plified for wide distributions, and the restored distribution presents significant uncertainties around the original one.

• The use of $\alpha = 1$ drastically reduces the amplification of noise in the wide distributions, significantly dropping the uncertainties of the restored size distribution with respect to the original one. Unfortunately, in this case the algorithm is not able to restore the sharp peak presented by the narrow distributions.

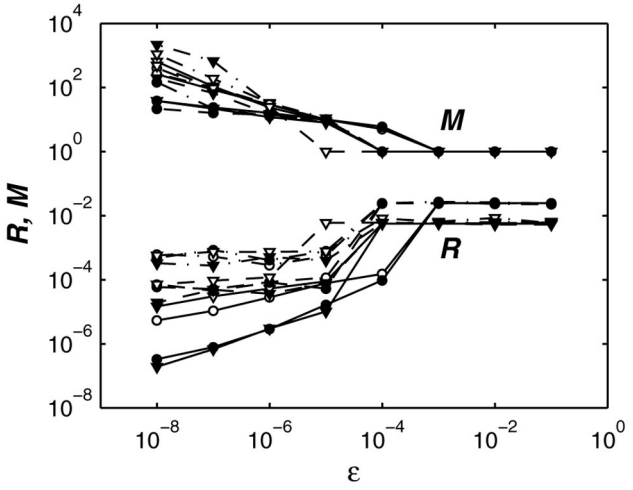

Fig. 9. Final residual R and number of iterations M as functions of the difference between two consecutive residuals ε. The size distributions have means $\overline{D} = 10$ μm (circles) and $\overline{D} = 60$ μm (triangles) and variance $\delta = 1.5$. The noise levels added to the power signal were 0% (solid lines), 1% (dashed lines), and 3% (dash–dotted lines). The values of α used in the restoration process were $\alpha = 0$ (filled symbols) and $\alpha = 1$ (open symbols).

• In all the simulated cases the total volume concentration of the restored size distribution does not significantly differ from the original volume concentration.

C. Bimodal Distributions and Independent Size Classes

To study the number of independent size classes that can be restored by use of each of the algorithms, in this subsection we focus on the algorithm's ability to capture the two peaks in an artificial size distribution with nonzero values just in two size classes separated by different numbers of empty size classes. The results are presented in Figs. 7 and 8. As expected, a larger separation (five size classes) is needed to detect the two peaks when the algorithm of Jianping *et al.*[10] ($\alpha = 1$) is used, whereas only two size classes are enough for the algorithm of Huang *et al.*[9] ($\alpha = 0$). The ability of these algorithms to actually capture the shape of the distribution is not discussed here because of the artificial nature of the size distribution. For Figs. 7 and 8, the simulations were run with no noise added to the signal and $\varepsilon = 10^{-6}$.

From these results it can be inferred that, in general, fewer than ten independent size classes can be resolved under optimal conditions with very low noise levels and narrow distributions that allow the use of small values of α. This agrees with the previous results obtained by Hirleman,[7] who studied the condition of the kernel matrix. Hirleman[7] showed that, for log-spaced sizes classes, more than 12 independent sizes are generally very difficult to obtain.

D. Condition of the Kernel Matrix and Error Estimation

The condition of the kernel matrix K_{ij} can be defined as

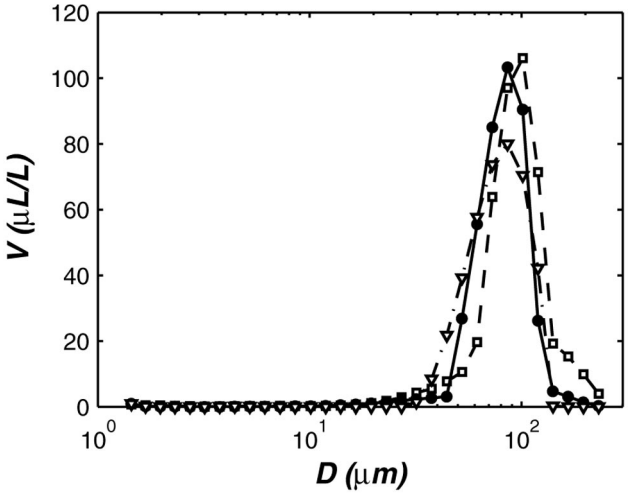

Fig. 11. Measured size distribution of ground silica retained between sieves with 53- and 74-μm apertures. The measured power signal was inverted with $\alpha = 0$ (open squares over dashed line), $\alpha = 1$ (open triangles over dash–dotted line), and $\alpha = 0.3$ (filled circles over solid line). The criterion to stop the iteration was $\varepsilon = 10^{-6}$ [condition (12)]. The residual, the total number of iterations, and the concentration were $R = 0.0319$, $M = 27$, and $V = 445$ for $\alpha = 0$, respectively; $R = 0.0203$, $M = 448$, and $V = 397$ for $\alpha = 1$, respectively; and $R = 0.0181$, $M = 57$, and $V = 414$ for $\alpha = 0.3$, respectively.

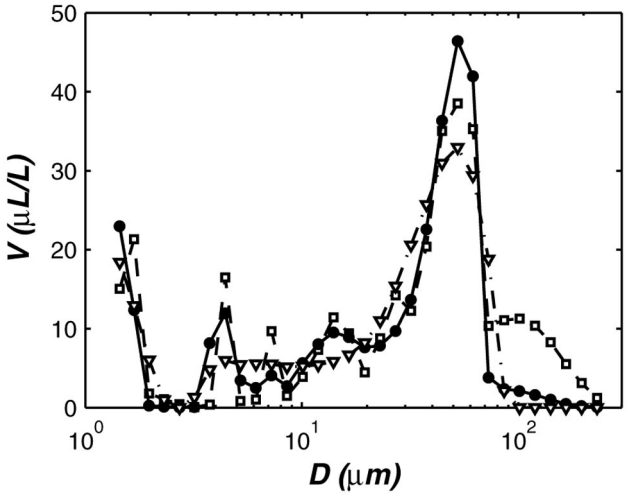

Fig. 12. Measured size distributions of raw ground silica. The measured power signal was inverted with $\alpha = 0$ (open squares over dashed line), $\alpha = 1$ (open triangles over dash-dotted line), and $\alpha = 0.3$ (filled circles over solid line). The criterion to stop the iteration was $\varepsilon = 10^{-6}$ [condition (12)]. The residual, the total number of iterations, and the concentration were $R = 0.0066$, $M = 299$, and $V = 332$ for $\alpha = 0$, respectively; $R = 0.0066$, $M = 424$, and $V = 291$ for $\alpha = 1$, respectively; and $R = 0.0045$, $M = 197$, and $V = 299$ for $\alpha = 0.3$, respectively.

$$\begin{aligned}\mathrm{cond}(K_{ij}) &= \|K_{ij}\|\,\|K_{ij}^{-1}\| \\ &= \left[\max\left(\frac{\|K_{ij}V_j\|}{\|V_j\|}\right)\right]\left[\min\left(\frac{\|K_{ij}V_j\|}{\|V_j\|}\right)\right]^{-1} \\ &\quad \text{with } V_j \neq 0, \end{aligned} \tag{16}$$

where $\|K_{ij}\|$ is any norm of the matrix K_{ij}. The condition of the kernel matrix that it is used to process the data of the LISST instruments, with the two-norm is $\mathrm{cond}(K_{ij}) = 9.1183 \times 10^8$.

The error associated with a restored solution $V_j^{M,N}$ can be bounded by use of the inequality

$$\frac{\|V_j - V_j^{M,N}\|}{\|V_j\|} \leq \mathrm{cond}(K_{ij})\,\frac{\|E_i - K_{ij}V_j^{M,N}\|}{\|E_i\|}. \tag{17}$$

Since K_{ij} is fix, the residual R defined in Eq. (11) is a bound to the error associated with restored solution. Taking squares, we obtain

$$\frac{\left[(V_j^{M,N} - V_j)(V_j^{M,N} - V_j)\right]}{(V_jV_j)} \leq [\mathrm{cond}(K_{ij})]^2\,R. \tag{18}$$

R is a measure of the difference between the measured and computed power, but when noise is present in the power signal, R does not decrease to zero, as shown in Figs. 9 and 10. Therefore, as $\mathrm{cond}(K_{ij})$ is large, the minimization of R does not necessary implies the minimization of the real and the restored size distribution difference. However, a large reduction of R will certainly imply a reduction on the restored size distribution difference. This is what the stopping criterion given by condition (12) expresses: If R does not decrease too much from one iteration to the next, the projection process should be stopped.

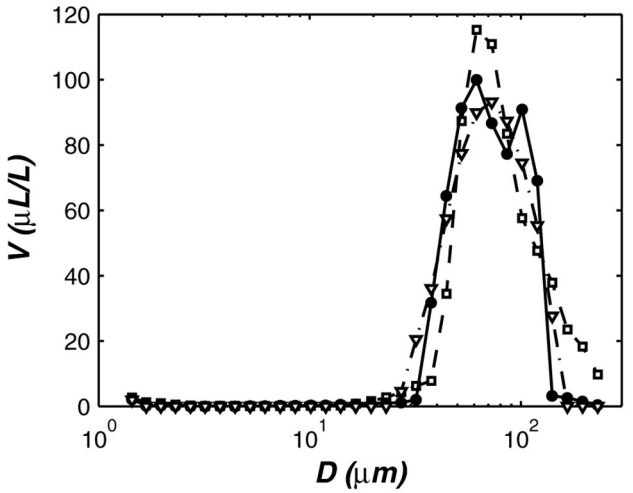

Fig. 13. Measured size distributions of a mixture of ground-silica particles retained between 53- and 74-μm aperture sieves and between 125- and 149-μm aperture sieves. The measured power signal was inverted with $\alpha = 0$ (open squares over dashed line), $\alpha = 1$ (open triangles over dash-dotted line), and $\alpha = 0.3$ (filled circles over solid line) and $\varepsilon = 10^{-6}$. The residual, the total number of iterations, and the relative volume were $R = 0.0387$, $M = 40$, and $V = 656$ for $\alpha = 0$, respectively; $R = 0.0170$, $M = 355$, and $V = 626$ for $\alpha = 1$, respectively; and $R = 0.0177$, $M = 549$, and $V = 629$ for $\alpha = 0.3$, respectively.

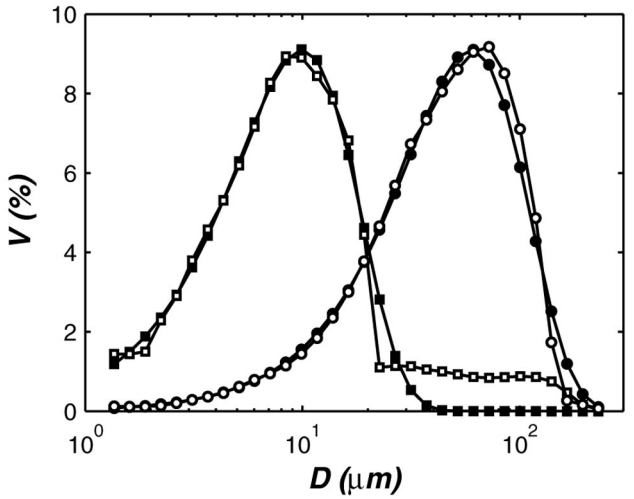

Fig. 14. Original (filled symbols) and restored (open symbols) size distributions with 3% noise added to the scattering power signal, with $\alpha = 0.3$. The criterion to stop the iteration was $\varepsilon = 10^{-6}$ [condition (12)]. The distributions have means $\overline{D} = 10\ \mu m$ (squares) and $\overline{D} = 60\ \mu m$ (circles) and width $\delta = 1.5$. The residual, the total number of iterations, and the relative volume were $R = 4.91 \times 10^{-4}$, $M = 34$, and $V = 1.02$ for $\overline{D} = 10\ \mu m$, respectively, and $R = 2.95 \times 10^{-4}$, $M = 17$, and $V = 1.00$ for $\overline{D} = 60\ \mu m$, respectively.

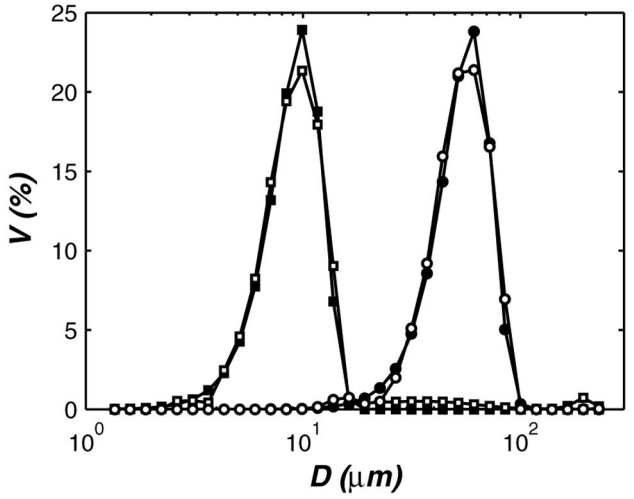

Fig. 15. Original (filled symbols) and restored (open symbols) size distributions with 3% noise added to the scattering power signal, with $\alpha = 0.3$. The criterion to stop the iteration was $\varepsilon = 10^{-6}$ [condition (12)]. The distributions have means $\overline{D} = 10\ \mu m$ (squares) and $\overline{D} = 60\ \mu m$ (circles) and width $\delta = 4$. The residual, the total number of iterations, and the relative volume were $R = 5.91 \times 10^{-4}$, $M = 131$, and $V = 1.04$ for $\overline{D} = 10\ \mu m$, respectively, and $R = 6.07 \times 10^{-4}$, $M = 124$, and $V = 1.01$ for $\overline{D} = 60\ \mu m$, respectively.

E. Convergence

The criterion to stop the iteration process used in all the simulations presented in this paper was $\varepsilon = 10^{-6}$. To determine this criterion, the convergence behavior of the algorithm was studied. The value of ε should be chosen as a balance between the size of the residual error and the number of iterations that are needed to reach the stopping condition.

In this analysis, no noise, 1% noise, and 3% noise were added to the power signals, and the same initial guess, an empty distribution, was used to make the results interpretation easier. This was repeated for different size distributions and for $\alpha = 0$ and $\alpha = 1$. The results for the final residual R and the number of iterations M plotted against ε are presented in Figs. 9 and 10. To produce these figures we used a different random noise distribution for each run and value of ε, allowing us to observe general trends and not just a particular case as if the same noise distribution were used for all the values of ε.

A jump in the plot is observed between $\varepsilon = 10^{-2}$ and $\varepsilon = 10^{-5}$ when the algorithm needs more than one iteration to satisfy the stopping condition. After this step, R and M change more or less linearly with ε if no noise is added to the signal. Under the presence of noise the residual R tend to reach an asymptotic value depending on the noise level and the value of α used. Basically the asymptotic value of the residual is proportional to the noise level in the signal, and, as could be expected, higher noise levels tend to have larger residuals. However, this is not exactly the case when we study distributions that present a sharp peak by using $\alpha = 1$. In this situation the inability of the algorithm to capture the peak tends to increase the number of iterations, and the residual continually decreases, although very slowly. For the same reason it can be seen in Fig. 10 that for 1% noise the residual value obtained with $\alpha = 0$ is smaller than the one obtained with $\alpha = 1$.

The residuals for different values of α are clearly separated if no noise is present in the signal, and $\alpha = 0$ always produce smaller residuals than $\alpha = 1$ with fewer iterations. However, if noise is present the results from different values of α cannot be clearly distinguished, and therefore the comparison between the qualities of restored distribution obtained with different values of α cannot be done in terms of the value of the residual R.

The value of ε to be selected is a compromise among the noise levels, the size distribution shape, the value of α that is being used, and the desired quality of the restored signal. As R is a bound only to the size distribution uncertainty, selecting a smaller value for ε will not necessary imply a more accurate restored distribution, especially for the smaller values of α. As a compromise solution for all the values of α and different size distributions, $\varepsilon = 10^{-6}$ was selected.

4. Practical Application of the Generalized Projection Algorithm

As presented in the previous section, the use of $\alpha = 1$ solves the uncertainties related to the presence of noise in the scattered light signal of wide distributions, but also reduces the high-resolution capabilities of the original projection algorithm ($\alpha = 0$).

The advantages of using an intermediate value of α can be observed in actual experimental data obtained

with a laser particle size analyzer. A LISST type B, developed by Sequoia, was used for the experiments presented here. It measures the laser beam diffraction pattern over 32 log-spaced ring-shaped detectors. Agrawal and Pottsmith[1] present a complete description of the instrument, and evaluations of the instrument made with natural and artificial particles can be found in the literature.[1,11,12] The LISST is a field instrument designed to measure concentration and size distribution in natural environments; therefore the evaluation that was done in our laboratory involved natural and artificial sediments. The experiments that are shown here were performed with ground silica. The different particle size samples were separated from the raw sediment by sieving. Although a deeper study of the instrument capabilities may involve the use of standard particles, the objective of the experiments presented here is to show the capabilities of the projection algorithm, and this can be achieved with the ground-silica particles.

The measured scattered light signal produced by a narrow distribution composed of particles retained between the sieves with apertures of 74 and 125 μm was inverted with $\alpha = 0$, $\alpha = 1$, and $\alpha = 0.3$ (Fig. 11). For all values of α the algorithm is able to identify the peak in the distribution. However, for $\alpha = 0$ a noise pattern similar to the one observed in Figs. 3 and 4 is observed at the larger sizes. For $\alpha = 1$ the peak width is increased, showing a nonnegligible concentration in a wider range. The peak's actual size is also underestimated, as was the case in the simulation presented in Fig. 6.

The retrieved distributions for particles in a wide size range (raw silica) with $\alpha = 0$, $\alpha = 1$, and $\alpha = 0.3$ are shown in Fig. 12. Again the use of $\alpha = 0$ introduces noise in the larger sizes, and when $\alpha = 1$ is used all the small peaks that exist in the size distribution are washed out. Here again $\alpha = 0.3$ gives a more realistic result.

A bimodal distribution composed of particles between 38- and 53-μm sieves and 125- and 149-μm sieves was retrieved again with three different values of α: 0, 1, and 0.3 (Fig. 13). With $\alpha = 1$ it is impossible to distinguish two peaks in the distribution. When $\alpha = 0$ is used, the size of the larger size peak is underestimated because of noise effects and the algorithm is not able to capture the two peaks. With $\alpha = 0.3$ two peaks are clearly observed.

Finally, for the sake of completeness and to allow comparison, Figs. 14 and 15 show the retrieved distributions from a scattered power signal with 3% noise added with $\alpha = 0.3$. The results, although not as good as the ones presented in Figs. 4 and 5, can still be considered satisfactory. These simulations also show that an intermediate value of α could give a good intermediate solution to the noise-resolution trade-off problem for a wide range of distributions as was shown by the experiments presented above.

5. Summary and Conclusions

The capabilities of the projection algorithms developed by Huang *et al.*[9] and Jianping *et al.*[10] in terms of noise-resolution trade-off were reviewed. None of them was able to solve the wide range of size distributions expected in natural environments under the presence of noise in the scattered light signal. As an alternative, we presented a generalization of the projection algorithm by introducing a parameter α that allows us to adjust the noise-resolution trade-off. This parameter α should be chosen to be as small as the size distribution and noise levels allow in order to obtain the highest size resolution possible in the restoring process. For the instrument used in the experiments presented here, the use of $\alpha = 0.3$ gave the best results in terms of stability and resolution for a wide range of size distributions.

This research was conducted under the Coastal Geosciences Program of the U.S. Office of Naval Research (grants N00014-03-1-0143 and N00014-01-1-0337). F. Pedocchi was also supported by a fellowship from the Organization of American States. This support is gratefully acknowledged. The authors would like to thank Juan E. Martín and Blake J. Landry for their useful suggestions when preparing the final version of this paper.

References

1. Y. C. Agrawal and H. C. Pottsmith, "Instruments for particle size and settling velocity observations in sediment transport," Mar. Geol. **168,** 89–114 (2000).
2. Y. C. Agrawal and H. C. Pottsmith, "Laser diffraction particle sizing in STRESS," Cont. Shelf Res. **14,** 1101–1121 (1994).
3. H. Gomi, "Multiple scattering correction in the measurement of particle size and number density by the diffraction method," Appl. Opt. **25,** 3552–3558 (1986).
4. E. D. Hirleman, "General solution to the inverse near-forward-scattering particles-sizing problem in multiple-scattering environments: theory," Appl. Opt. **30,** 4832–4838 (1991).
5. H. Mühlenweg and E. D. Hirleman, "Laser diffraction spectroscopy: Influence of particle shape and shape adaptation technique," Part. Part. Syst. Charact. **15,** 163–169 (1998).
6. T. Matsuyama, H. Yamamoto, and B. Scarlett, "Transformation of diffraction pattern due to ellipsoids into equivalent diameter distribution for spheres," Part. Part. Syst. Charact. **17,** 41–46 (2000).
7. E. D. Hirleman, "Optimal scaling of the inverse Fraunhofer diffraction particle sizing problem: the linear system produced by quadrature," Part. Part. Syst. Charact. **4,** 128–133 (1987).
8. J. B. Riley and Y. C. Agrawal, "Sampling and inversion of data in diffraction particle sizing," Appl. Opt. **30,** 4800–4817 (1991).
9. T. S. Huang, D. A. Barker, and S. P. Berger, "Iterative image restoration," Appl. Opt. **14,** 1165–1168 (1975).
10. W. Jianping, X. Shizhong, Z. Yimo, and L. Wei, "Improved projection algorithm to invert forward scattered light for particle sizing," Appl. Opt. **40,** 3937–3945 (2001).
11. J. W. Gartner, R. T. Cheng, P. Wang, and K. Richter, "Laboratory and field evaluations of the LISST-100 instrument for suspended particle size determinations," Mar. Geol. **175,** 199–219 (2001).
12. P. Traykovski, R. J. Latter, and J. D. Irish, "A laboratory evaluation of the laser in situ scattering and transmissometery instrument using natural sediments," Mar. Geol. **159,** 355–367 (1999).